Applied Microbiology and Biotechnology (2025) 109:55
https://doi.org/10.1007/s00253-025-13437-x

METHODS AND PROTOCOLS

Ultra-sensitive immunosensing of snake venom by functionalized Sm-Co doped antimony-tungstate

Rimsha Batool[1] · **Sana Shaheen**[1] · **Batool Fatima**[1] · **Dilshad Hussain**[2] · **Ukasha Jawad**[3] · **Ayub Alam**[4] · **Muhammad Najam-ul-Haq**[5]

Received: 18 May 2024 / Revised: 27 November 2024 / Accepted: 18 February 2025

Abstract

Snake venom has long-term physiological effects on survivor's life. An electrochemical immunosensor based on samarium-cobalt-doped antimony tungstate (Sb_2WO_4@Sm-Co) is developed via a solvothermal method to detect snake venom antigens (SVA). The fabricated nanospheres are functionalized with carboxyl groups to enhance the linkage of the 3-mercaptopropionic acid linker (3-MPA). This modification increases the conjugation of antivenom polyvalent antibody with the nanomaterial on a glassy carbon electrode (Sb_2WO_4@Sm-Co-COOH-MPA-Ab/GCE). The modified nanospheres are characterized by UV–VIS spectroscopy, Fourier transform infrared spectroscopy (FTIR), scanning electron microscopy (SEM), transmission electron microscopy (TEM), and energy dispersive X-ray spectroscopy (EDS). The electrochemical performance of formulated immunosensor for antigen sensing is tested by cyclic voltammetry (CV), electrochemical impedance spectroscopy (EIS), differential pulse voltammetry (DPV), linear sweep voltammetry (LSV), and chronoamperometry. This developed immunosensor has a wide linear range of 5–30 ng/mL with LODs of 0.08 ng/mL and 0.1 ng/mL from DPV and LSV, respectively. The amperometric immunosensor increases the tested antibody's loading capacity and accelerates the electron transfer rate. The analytical parameters reveal that this immunosensor is ultrasensitive, stable, reproducible, and selective for measuring SVA and can have potential applications in diagnostic clinics.

Key points

- *The hierarchical Sb_2WO_4@Sm-Co-COOH NPs were synthesized through a one-step solvothermal method*
- *Monitoring the effect of doping Sm and Co on the characteristics of Sb_2WO_4*
- *MPA-linked IgG antibodys-based immunosensor was synthesized with good dispersity and high surface functional groups for capturing SVAs*

Keywords Snake venom · Biosensors · Antivenom · Russel's Viper *(Daboia russelii)* · Impedimetric immunosensor · IgG antibody · 3-mercaptopropionic acid linker

✉ Batool Fatima
batoolfatima@bzu.edu.pk

[1] Department of Biochemistry, Bahauddin Zakariya University, Multan 60800, Pakistan

[2] International Center for Chemical and Biological Sciences, HEJ Research Institute of Chemistry, University of Karachi, Karachi 75270, Pakistan

[3] Department of Biomedical Engineering, University of Engineering and Technology, Narowal Campus, Lahore, Pakistan

[4] Department of Chemistry, The Islamia University, Bahawalpur, Pakistan

[5] Institute of Chemical Sciences, Bahauddin Zakariya University, Multan 60800, Pakistan

Introduction

Immunoglobulins stop the growth or emergence of pathogenic bacteria, viruses, parasites, and fungi (L. Lee et al. 2021). The interactions between immunoglobulin and antigen usually occur through paratopes and epitopes, which depict the location of the bound antigen. Acute exposure to an immunogen or pathogen is diagnosed using IgM antibodies linked to a primary immune response. The sensitivity of the target molecule accounts for relatively low concentrations of circulating IgD in serum and its short serum half-life (Schroeder Jr and Cavacini 2010). IgA shields the mucous membranes from bacteria, viruses, and toxins by neutralizing or preventing their attachment. One of the effective

Published online: 03 March 2025

immunoglobulins is IgE, which is linked to allergic reactions, hypersensitivity, and the body's reaction to pathogenic parasitic infestations (Li et al. 2020).

With over 80% of all serum immunoglobulins, IgG is regarded as the most prevalent class (Megha and Mohanan 2021). IgG serum half-life is the longest and most investigated among all immunoglobulin isotypes. IgG2 and IgG4 antibodies are linked to polysaccharide antigens, while IgG1 and IgG3 are generated in response to protein antigens. IgG antibodies support an immune response by neutralizing viruses and harmful substances (Schroeder Jr and Cavacini 2010). B cells produce monoclonal antibodies (mAbs) specific for targeting particular antigens (Lu et al. 2020). Pathogens can be neutralized, opsonized, subjected to antibody-dependent cellular cytotoxicity (ADCC), or agglutinated by antibodies. Antibodies wrap up infections to aid in their opsonization or breakdown. The role of neutrophils and macrophages is to phagocytose pathogens coated with antibodies (Abbas et al. 2012). Antigen–antibody complexes decipher the intricate antigen–antibody interactions and clarify their molecular recognition. Many allergies and autoimmune disorders develop antigen–antibody complexes. Antibodies are thus the naturally occurring biological sensors in disease diagnosis and treatments. Antigen presentation and processing are the two immune responses of antigen binding to antibodies, which cause alteration in antigen's characteristics (Kapingidza et al. 2020).

Enzyme-linked immunosorbent assay (ELISA), immunoprecipitation, enzyme immunoassay (EIA), flow cytometry, immunohistochemistry (IHC), and immunocytochemistry employ antibodies (Rhiel and Becker 2021). ELISA and EIA are quantitative techniques that use antigen–antibody reactions for color change via enzyme-linked conjugate and enzyme substrate to determine the presence and concentration of molecules in biofluids (Aydin 2015). IHC is a potent technique to locate antigens in formalin-fixed, paraffin-embedded (FFPE) tissues (Schacht and Kern 2015). ELISA's sensitivity, specificity, and ease of use make it one of the most widely used diagnostic techniques. Its limit of detection ranges from 0.1 to 1.5 ng/ml. The quick identification of biological samples is hindered by the fact that ELISA typically achieves a detection time of 2–4 h (Chen et al. 2023). Immunoprecipitation produces highly pure immune complexes from homogenized tissues or cell lysates. This technique has the disadvantage of detecting non-specific proteins (DeCaprio and Kohl 2020). The EIA makes it possible to find highly minute amounts of antigens in a sample, including proteins, peptides, hormones, and antibodies (Ahsan 2022). Risks associated with EIA include overestimating population susceptibility, producing false negative results, and the high cost (Lutz et al. 2023). Flow cytometry provides fast and quantitative analysis of different parameters of cell populations via a single cell (Manohar et al. 2021). Inadequate data analysis, efficiency, and specimen quality are issues (Brestoff and Frater 2022). Immunohistochemistry offers high-throughput multiplex staining and standardized quantitative analysis for highly reliable, effective, and economic tissue research. Some disadvantages of this technique are that it can only label one marker from the tissue section, and there is substantial variability (Tan et al. 2020). The diagnostic cytopathology employs immune-cytochemical reactions. However, incorrect diagnosis occurs through interpretation errors, false-positive or false-negative data, or both (Leonardo et al. 2020).

Nanotechnology can help better identify diseases and treat various ailments (Kirtane et al. 2021). The magnetic, optical, chemical, physical, and electrical features of diverse nanomaterials in chemo/biosensing platforms can target various analytes (Kumar et al. 2020; Shen et al. 2021). The electrochemical biosensors offer mobility, affordability, selectivity, and the potential for downsizing. The nanomaterials have fueled the growth of biosensors in the last two decades (Leote et al. 2022). The reversible and selective interaction of the sensor with the analyte produces measurable chemical parameters to determine its concentration. Electrochemical biosensors are sensitive, selective, and fast. They detect viruses, i.e., coronavirus, dengue virus, human immunodeficiency virus (HIV), hepatitis B virus (HBV), and hepatitis C virus (HCV) (Orooji et al. 2021).

Antimony (Sb) has potential in biomedical research and clinical diagnosis. "Sb_2O_4/rGO"-based sensors determine real-time nitric oxide molecules emitted from normal skin cells and tumor cells (Deng et al. 2021; Lee et al. 2020). Sm is used as a dopant to enhance the functioning of conductometric gas sensors (Rasouli Jamnani et al. 2019). "SiO_2-Sm_2O_3" NPs have more porosity when the samarium ion is added. Additionally, it increased the quantity of weak Lewis acid sites and had the potential to significantly improve the biological activity of the produced nanomaterial (Blasques et al. 2020). High catalytic activity, low cost, and good stability are reported for "Co_3O_4" (Zhuang et al. 2019). Antimony tungstate (Sb_2WO_6), a typical n-type semiconductor having an appropriate band gap structure, has been extensively researched in the fields of gas sensors and catalytic processes (Rafiq et al. 2020).

With the broad applications and chemical-electrochemical characteristics of the mentioned elements, a signal-enhancing immunosensor based on samarium-cobalt doped antimony tungstate (Sb2WO4@Sm-Co) is constructed to achieve ultrasensitive detection of an antigen–antibody complex with snake venom. It has abundant functional groups for the attachment of biomolecules. EDC/NHS act as indispensable cross-linkers; their bioconjugation changes the composite's surface to bind amine-reactive antibody groups. Nanocomposite is functionalized with a 3-mercaptopropionic acid (3-MPA) linker to avoid aggregation and polymerization and to couple antibodies covalently. The antibody would not be randomly oriented on NPs, which is effective for the antigen binding sites' accessibility. According to the literature survey, this is the first formulated immunosensor for ultrasensitive snake venom antigen (SVA) detection through electrochemical immunosensing.

Materials and methods

Chemicals and reagents

Sodium tungstate dihydrate ($Na_2WO_4.2H_2O$, ≥ 99%), deionized water (99%), ethanol (C_2H_6O, 100%), antimony trichloride ($SbCl_3$, 95%), samarium nitrate ($SmNO_3$, 85%), cobalt nitrate hexa-hydrate ($Co(NO_3)_3.6H_2O$, 98%), sodium hydroxide (NaOH, 99%), ammonia (NH_3, 85%), distilled water (99%), 3-mercaptopropionic acid ($C_3H_6O_2S$, 98%), 1-ethlyl-3-(3-dimethylaminopropyl) carbodiimide ($C_8H_{17}N_3$, 95%), and N-hydroxysuccinimide ($C_4H_5NO_3$, 95%), Polyethylene glycol (PEG) were purchased from Sigma-Aldrich. The anti-venom polyvalent antibodies (IgG) were provided by the National Institute of Health Islamabad Pakistan, and it was prepared against a venomous snake named Russell's viper (Daboia russelii), which was collected from a snake charmer.

Synthesis of nanomaterial

A one-step solvothermal method was slightly modified from earlier studies to synthesize Sb_2WO_4@Sm-Co (S. Chen et al. 2018; Zhang et al. 2022). The solution contained 1 mmol of $Na_2WO_4·2H_2O$ in 8 mL deionized water. Solution II was 2 mmol $SbCl_3$ in 8 mL ethanol. Solution II was added to solution I to obtain a yellowish mixture. This solution was mixed with 0.2 mmol each of $SmNO_3$ and $Co(NO_3)_3·6H_2O$. NaOH/HNO_3 (1 mL) solution was added to the suspension for attaining pH 2 and stirred for 30 min. The obtained solution was stirred for 10 min and put into a 20 mL Teflon-lined stainless-steel autoclave for a 24-h hydrothermal reaction at 180 °C. The product was collected by washing with deionized water and 100% ethanol. The reaction mechanism is shown in the following equations.

$$SbCl_3 + 3C_2H_5OH \rightarrow Sb(OCH_2CH_3)_3 + 3HCl \quad (1)$$

$$Sb(OCH_2CH_3)_3 + Na_2WO_4.2H_2O + 3H_2O \rightarrow Sb(OH)_3 + 3C_2H_5OH + 2NaOH + H_2WO_4 \quad (2)$$

$$Sb(OH)_3 + H_2WO_4 + NaOH \rightarrow Na[Sb(OH)_6] + H_2O + WO_4 \quad (3)$$

Functionalization

For attachment of the linker via its SH group, this composite must include an efficient functional group containing hydroxyl groups. Citric acid was used to functionalize the NPs with COOH groups. 0.01 g dried NPs were suspended in 1 mL water, followed by adding 0.01 g citric acid, and stirred for 90 min at 90 °C. The unreacted content was removed by washing it with distilled water. The functionalized NPs were dried in an oven (Ghafoor and Ata 2017). The whole scheme of nanocomposite formulation is shown in Scheme 1.

Conjugation of Sb_2WO_4@Sm-Co-COOH with antivenom polyvalent antibodies

The 3-mercaptopropionic acid (3-MPA) linker with two carbon atoms between COOH and SH groups was used to modify Sb_2WO_4@Sm-Co-COOH. 1 mL COOH-modified nanomaterial was treated with 100 µL of 20 mM 3-MPA for 96 h at 800 rpm and 25 °C. After three centrifugation cycles at 6000 rpm for 15 min, the modified NPs were resuspended in 500 µL ultrapure water. The bioconjugation was made through EDC/NHS, wherein 100 µL ligand-modified NPs were combined with 10 µL of 50 µM EDC and left for 30 min. It was further stirred for 30 min at 150 rpm after adding 10 µL of 75 µM NHS. The solution was stirred for 30 min by adding 25–30 ng/mL antivenom polyvalent antibodies (whole IgG), which require incubation at 37℃. The antibodies were immobilized through amino groups to create a pre-activated carboxylic acid amide bond (EDC/NHS). The material was finally centrifuged for 20 min, the supernatant was discarded to remove unreacted functional groups of glutaraldehyde in the EDC/NHS complex that were not bound to the antibody, and the pellet was then resuspended in 100 µl of 1% PEG for functionalizing nonantibody coated areas (Oliveira et al. 2019). This guarantees that the carboxyl-terminal group of 3-MPA will experience the activation of the crosslinking molecules. The thiolation reaction occurred through bonding SH-NPs, generating a densely packed thiolated 3-MPA self-assembled monolayer (SAM). Resultantly, the formation of the immunosensor (Sb2WO4@Sm-Co-COOH-MPA-Ab) occurs, as illustrated in Scheme 2.

Fabrication of immunosensing platform

A glassy carbon electrode (GCE) was polished by polishing cloth and sonicated for 20 min in ethanol to remove

Scheme 1. Schematic representation of the hydrothermal formation of Sb_2WO_4@Sm-Co-COOH. Synthesis of hydroxyl group containing Antimony tungstate NPs doped with Samarium and cobalt. Citric acid was added to functionalize these fabricated NPs with Carboxyl groups, which are required to bind the linker

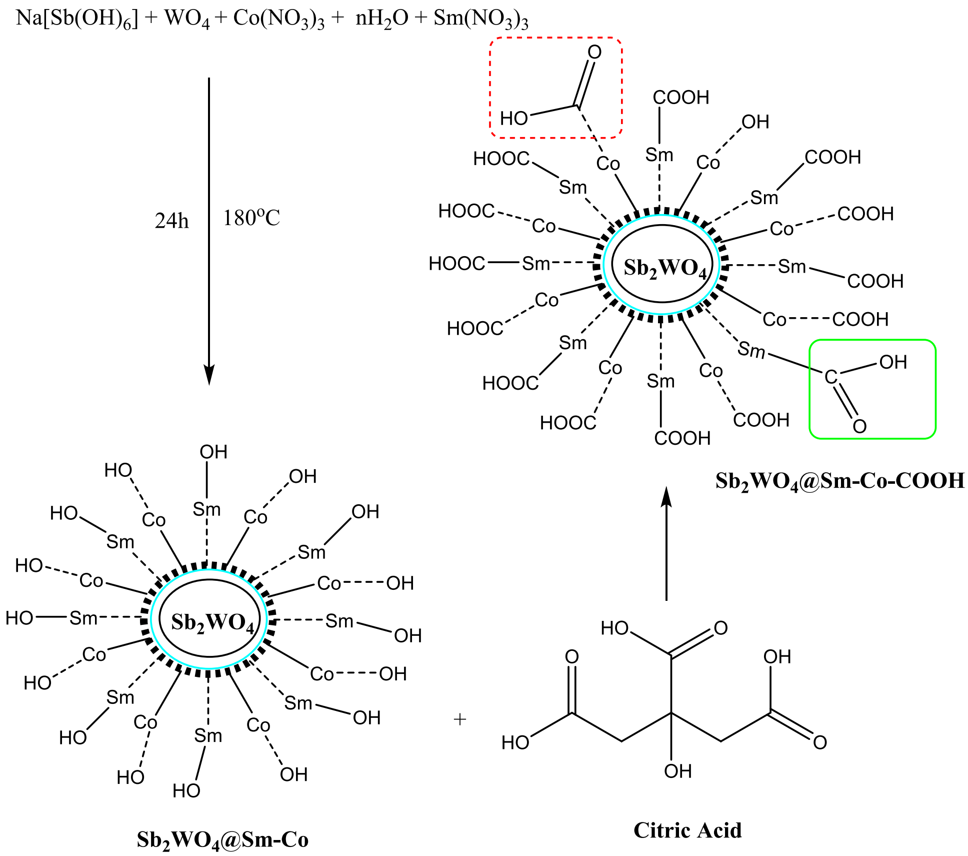

the contaminants. The electrode was then washed with distilled water, and a 5 µL suspension of immuno-nanomaterial (Sb_2WO_4@Sm-Co-COOH-MPA-Ab) was deposited on GCE. It was then allowed to dry at room temperature and maintained at 4 °C before analysis.

The modified working electrode was used to detect SVA, which had a lifespan of a few weeks.

Electrochemical sensing of snake venom

Electrochemical experiments were performed using the three-electrode system Potentiostat/ Galvanostat device at 25 °C. Immuno-sensing was employed to detect SVA in PBS solution via the electrochemical cell, which had a counter electrode (platinum wire), reference electrode (Ag/AgCl), and working electrode (GCE). The electrochemical behavior of Sb_2WO_4@Sm-Co-COOH-MPA-Ab was analyzed with cyclic voltammetry (CV). Snake venom solutions of varied concentrations and pH were analyzed via DPV, LSV, EIS, and chronoamperometry at room temperature.

Results

Characterization of Sb_2WO_4@Sm-Co-COOH

The structure of synthesized nanomaterial is investigated via scanning electron microscopy (SEM). The image exhibits a densely packed layer of spherical and rod-shape NPs, which showed agglomerated morphology (Fig. 1A). The histogram in Fig. 1B indicates that the solid sphere Sb_2WO_4@Sm-Co-COOH has a size distribution of 20–36 nm. There are numerous, easily noticeable micropores on the surface of the thin layer. The addition of Sm and Co extensively regulates the morphology of the Sb_2WO_6 matrix, and pure Sb_2WO_6 exhibits an evident layered microsphere structure. The size distribution and consistent density of NPs are visible in TEM, and micrographs illustrate their specific surface area and uniformity (Fig. 1C). The synthetic Sb_2WO_4@Sm-Co-COOH is dispersed as small particles with an average diameter of ~ 25 nm.

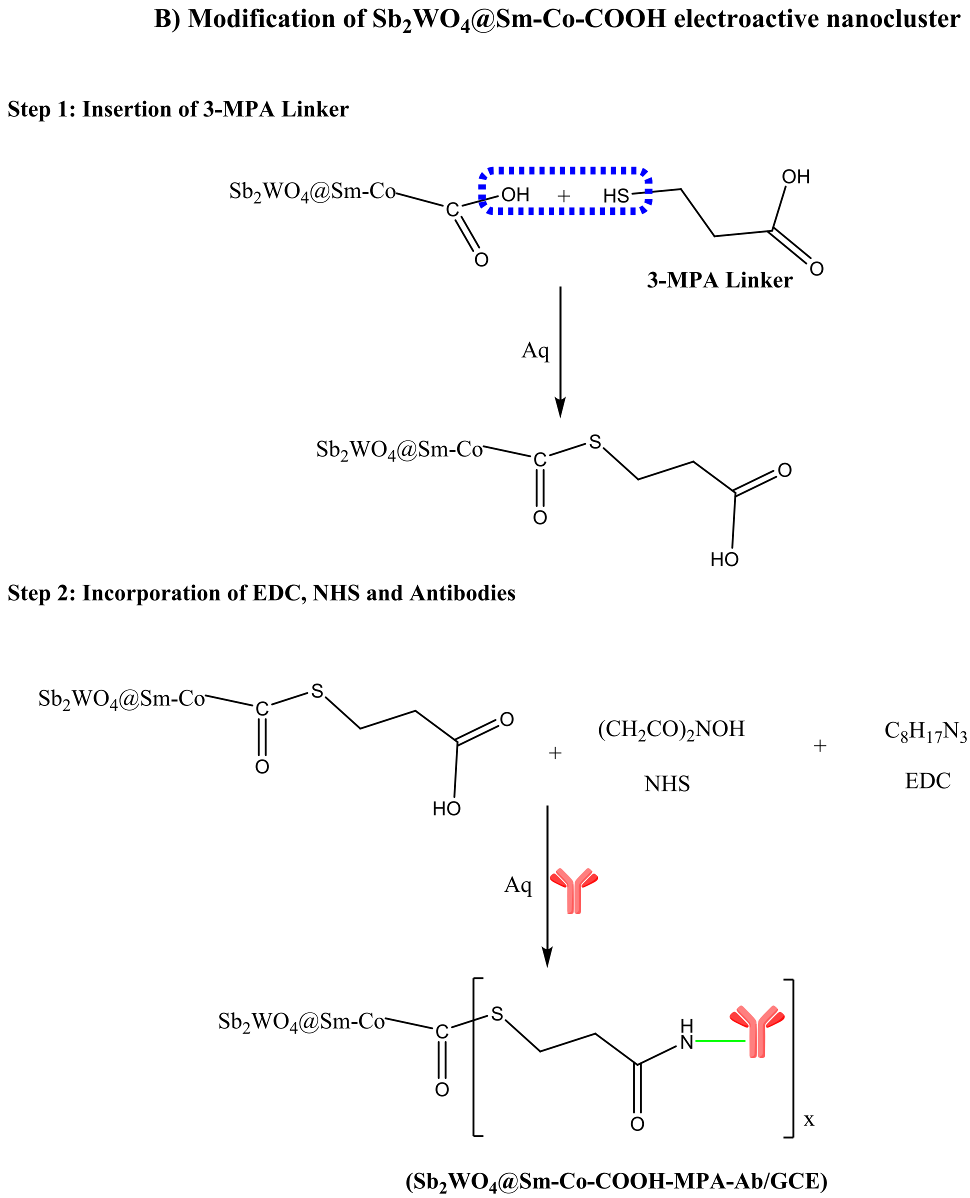

Scheme 2. Schematic representation for the formation of Immunosensor (Sb_2WO_4@Sm-Co-COOH-MPA-Ab). Step 1: thioester bond between COOH functionalized NPs and 3-MPA linker. Step 2: Covalent immobilization of Antibody with NPs via NHS and EDC cross-linkers

Citric acid with three carboxyl groups fills these gaps and enhances the material homogeneity and specific surface area. The energy dispersive spectrometry (EDS) spectra reveal the distribution of Sb, Sm, Co, W, and COOH. The fabricated Sb_2WO_4@Sm-Co-COOH consists of uniformly distributed 16.53% COOH, 9% Co, 40% Sb, 1.24% Sm, and 32.42% tungstate (Fig. 1D).

UV–visible spectroscopy verifies the NP production by assessing the collective oscillations of the conduction band and electrons in response to electromagnetic waves and detecting plasmon resonance. This provides initial details of NP aggregation, stability, size, and structure (Mourdikoudis et al. 2018). Sb_2WO_4@Sm-Co has an absorption wavelength of 214 nm due to its large band gap, which results in limited UV light absorbance. With a small band gap, the range of absorption curve for Sb_2WO_4@Sm-Co-COOH extended to 216 nm. In visible light, functionalization showed a broad absorption spectrum (Fig. 2A).

$$E = \frac{1240}{\lambda(nm)}eV \tag{4}$$

Using Eq. 1, the calculated band gaps for Sb_2WO_4@Sm-Co and Sb_2WO_4@Sm-Co-COOH are 5.79 eV and 5.74 eV, respectively, indicating no significant change in the band gap.

The materials' infrared Fourier transform spectroscopy (FTIR) was recorded between the mid-infrared range of 500 and 4000 cm^{-1} to investigate the functional groups (Rabiei et al. 2020). Figure 2B depicts the peaks

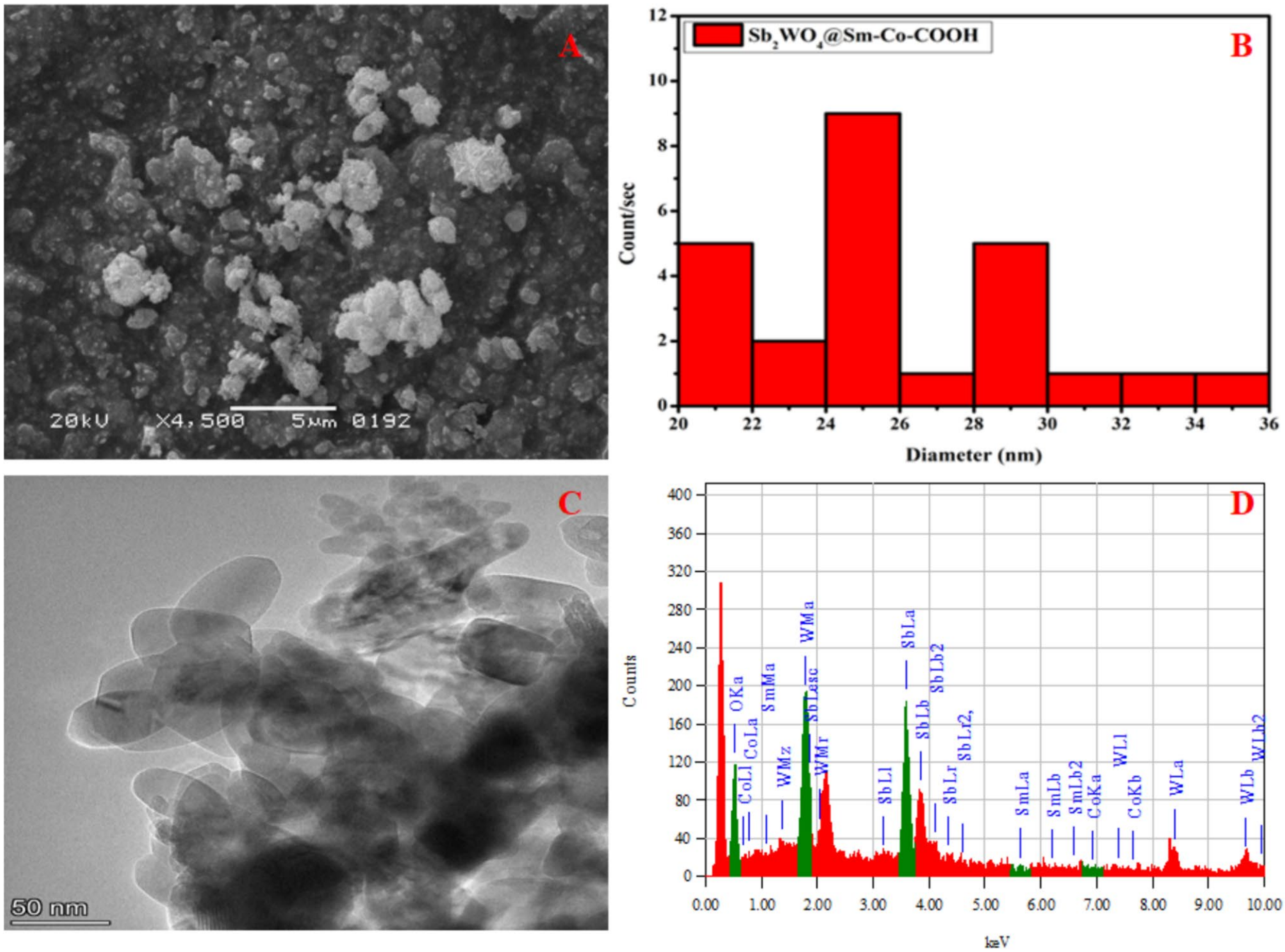

Fig. 1 **A** SEM image, **B** Histogram, **C** TEM image, and **(D)** EDS spectrum of Sb_2WO_4@Sm-Co-COOH

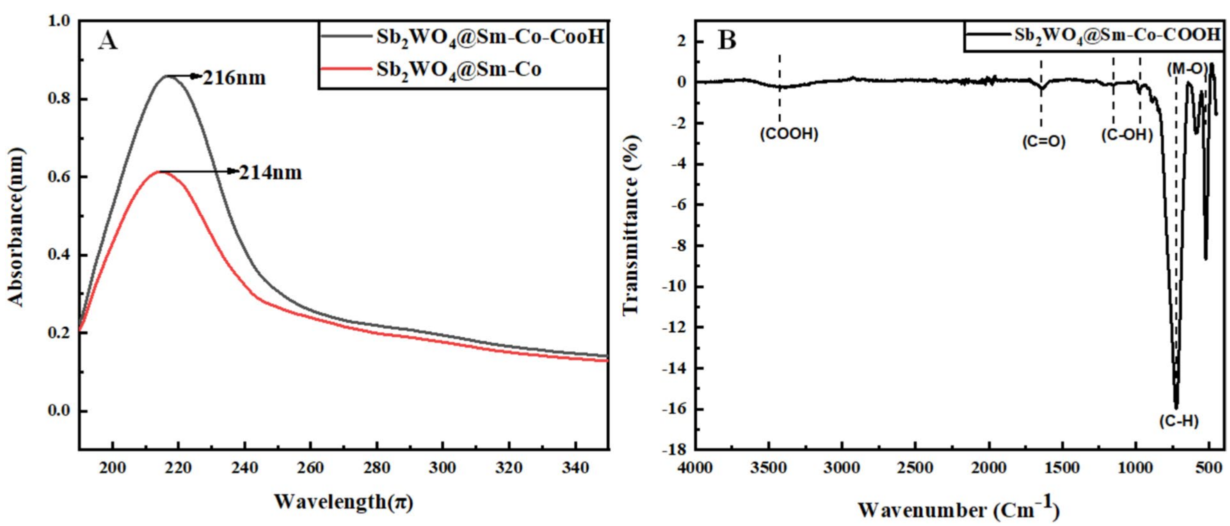

Fig. 2 **A** UV spectra of Sb_2WO_4@Sm-Co (14 nm) and Sb_2WO_4@Sm-Co-COOH (16 nm), and **(B)** FTIR spectrum of Sb_2WO_4@Sm-Co-COOH indicating C-H, C–OH, C = O, COOH and M–O bonds

of Sb_2WO_4@Sm-Co-COOH at 3430 cm^{-1} (S. Chen et al. 2018; Zhang et al. 2022), 1000–1150 cm^{-1}, and 750 cm^{-1}. The absorption at 3350 cm − 1 further validated the successful functionalization of nano-spheres with carboxylic acid. The M–O bond is responsible for the distinctive absorption band visible in the NP spectra at 500 cm^{-1}.

Analytical performance of MPA-Ab linked Sb_2WO_4@Sm-Co-COOH

The voltammetric analysis of Sb_2WO_4@Sm-Co-COOH-MPA-Ab was investigated by modified GCE immersed in 0.1 M KCl solution. The electrochemical activity of the immuno-electrode was analyzed using CV with a potential range of −0.4 to 1.0 V and a scan rate of 30 mVs^{-1}. Figure 3A depicts no oxidation–reduction peaks on bare GCE, while Sb_2WO_4@Sm-Co-COOH-MPA-Ab /GCE shows oxidation peaks at 0.5 V and 35 µA current. Figure 3B depicts that Sb_2WO_4@Sm-Co-COOH-MPA-Ab is stable and conductive.

The performance of electrochemical sensors can be directly impacted by the surface area, roughness, and porosity of electrodes (Lahcen et al. 2020). To ascertain the electrochemically active surface area, ECSA was investigated in $K_4[Fe(CN)_6]^{3-/4-}$ (0.1 mM) and KCl (0.1 M) solutions in a 1:1 ratio. Under the specified experimental conditions, this study measures the maximum electrochemical activity of Sb_2WO_4@Sm-Co-COOH-MPA-Ab at a scan rate of 70 mV/s and a maximum current of 0.015 mA. Figure 3C illustrates how the current decreases with the decrease in scan rate to suggest a reduction in the electrochemical reaction. ECSA results showed the highly rough and porous nature of the modified electrodes. Figure 3D depicts the line graph of ECSA, and the equation to calculate ECSA is mentioned below:

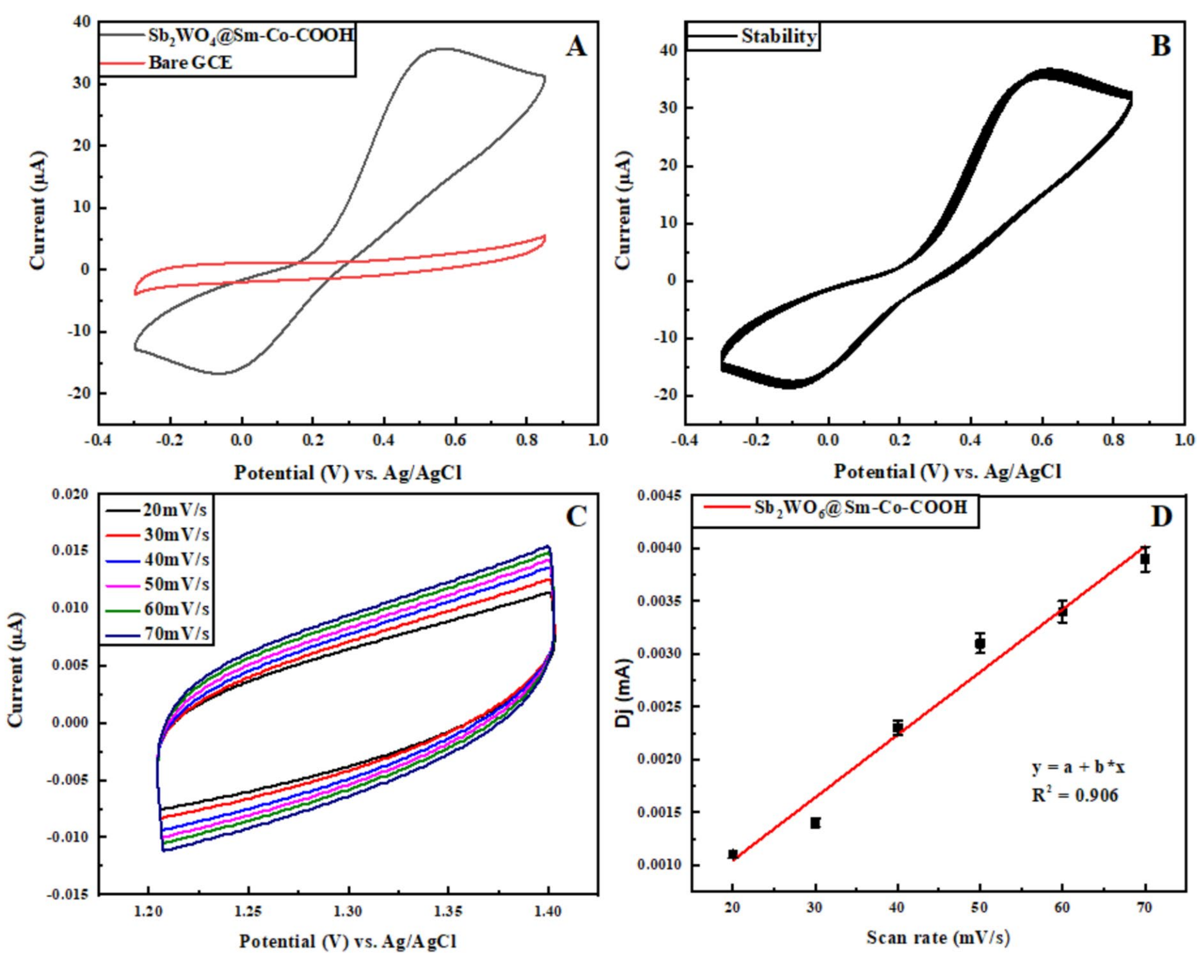

Fig. 3 **A** Cyclic voltammetry for the conductivity of Sb_2WO_4@Sm-Co-COOH and bare electrode in 0.1 M $K_4[Fe(CN)_6]^{3-/4-}$ & 0.1 M KCl solution, **B** Stability of Sb_2WO_4@Sm-Co-COOH by conducting 50 cycles in 0.1 M $K_4[Fe(CN)_6]^{3-/4-}$ & 0.1 M KCl solution, and (**C**) ECSA of Sb_2WO_4@Sm-Co-COOH in 0.1 M $K_4[Fe(CN)_6]^{3-/4-}$ & 0.1 M KCl solution, at scan rate of 20mVs^{-1}–70mVs^{-1}) (**D**) The corresponding line graph of ECSA with determination coefficient value of 0.906

$$ECSA = \frac{Slope \times 1000}{2} \quad (5)$$

ECSA calculated for Sb_2WO_4@Sm-Co-COOH is 0.145.

Roughness factor

The roughness factor (Rf) relies on the size of the electrode and the number of redox sites on the electrode surface. It is the ratio of the surface area of the modified electrode to the surface area of bare GCE. Rf of Sb_2WO_4@Sm-Co-COOH modified electrode is calculated using the formula:

$$R_f = \frac{A_2}{A_1} \quad (6)$$

A_1 is the surface area of the bare electrode, i.e., 0.073, and A_2 is the surface area of the Sb2WO4@Sm-Co-COOH-MPA-Ab modified electrode, i.e., 0.145 cm^2. The roughness factor is found to be 1.98.

Heterogeneous electron transfer (k°)

The k° measurements are performed for the Sb_2WO_4@Sm-Co-COOH modified and bare electrodes. The heterogeneous electron transfer rate constant on a modified electrode is examined using electrochemical impedance spectroscopy. Bare GCE shows a substantial semicircle with a surface area of 0.073 cm^2. Compared to imino-nanomaterial, which has an Rct of 22,018 Ω, its Rct value is 27,659 kΩ. The huge surface area of Sb_2WO_4@Sm-Co-COOH-MPA-Ab was measured as 0.145 cm^2. The following formula is used by EIS to determine the standard heterogeneous rate constant (k°).

$$k^{\circ} = \frac{RT}{F^2 R_{ct} A C} \quad (7)$$

where A is the electrode's surface area, C is the concentration of potassium ferrocyanide ($K_4Fe(CN)_6$) solution used as a redox probe, T is the temperature, F is the Faraday constant, Rct is the charge transfer resistance, and R is the gas constant. The k° value for the modified electrode is 8.1×10^{-7}, whereas for the bare electrode, it is 1.31×10^{-6}. The k° values for both electrodes indicate how well electron transfer mechanisms work at their surfaces.

Differential pulse voltammetry (DPV) analysis

DPV was used to examine the electrochemical process of the altered electrode. The current variation was shown as a function of potential during the DPV measurement. The electrochemical behavior of the immunosensor is also monitored using DPV at various pH (6.8, 7.0, 7.2, 7.4, 7.6, and 7.8). Therefore, pH 7.4 ensures the immunosensor operates as intended by preserving its physiological properties. The generated current varies with pH (Fig. 4A). The pH variation affects SVA's electrochemical activity on the fabricated immunosensor surface. Figure 4B depicts the line graph of DPV at various pH ranges. A range of snake venom concentrations are tested to see how the immunosensor responds. The highest oxidation reaction between snake venom and Sb_2WO_4@Sm-Co-COOH-MPA-Ab occurs at 30 ng/mL with the maximum current response (Fig. 4C). A modest decrease in response to 3.75 µA is seen as the concentration drops to 25 ng/mL. The current responses are 3.3 µA, 3.0 µA, 2.7 µA, and 2.5 µA, respectively, at 20 ng/mL, 15 ng/mL, 10 ng/mL, and 5 ng/mL concentrations. Its linearity (R^2) is 0.99 (Fig. 4D).

Linear sweep voltammetry (LSV) analysis

The potential is swept linearly over time, and LSV measures the current response. Experiments using LSV were conducted in the potential range of −1 to + 1 V. The current peaks at different pH ranges (7.4, 7.6, 7.2, 7.8, 7.0, and 6.8) are 5 µA, 4 µA, 3.5 µA, 3 µA, 2.5 µA, and 2 µA, subsequently. There is a linear correlation between the pH of the solution and the current response (Fig. 5A and B). LSV evaluates oxidation of snake venom at different quantities, i.e., 30 ng/mL, 25 ng/mL, 20 ng/mL, 15 ng/mL, 10 ng/mL, and 5 ng/mL. The current responses at various concentrations are 5 µA, 4.4 µA, 4 µA, 3.5 µA, 3 µA, and 2.5 µA, respectively is represented in Fig. 5C. Every peak potential is constant at 0.1 V, and the linearity (R^2) is ~ 0.99 (Fig. 5D).

Limit of detection (LOD)

LOD is the least detectable quantity of analyte, i.e., snake venom. It is determined by the following formula:

$$LOD = 3\frac{s}{m} \quad (8)$$

where m denotes the slope and s is the standard deviation. LODs for DPV and LSV are calculated as 0.08 ng/mL and 0.1 ng/mL, correspondingly.

Impedimetric detection of target antigen in EIS mode

Identifying the interface-related characteristics of fabricated electrodes could be facilitated by the use of electrochemical impedance spectroscopy (EIS) (Hu et al. 2021). Determining the resistance on the electrode material and between the electrode and the analyte is another crucial task for the EIS approach (Saxena et al. 2022). Using EIS with a frequency range of 0.01 Hz, the modified electrodes' charge-transfer

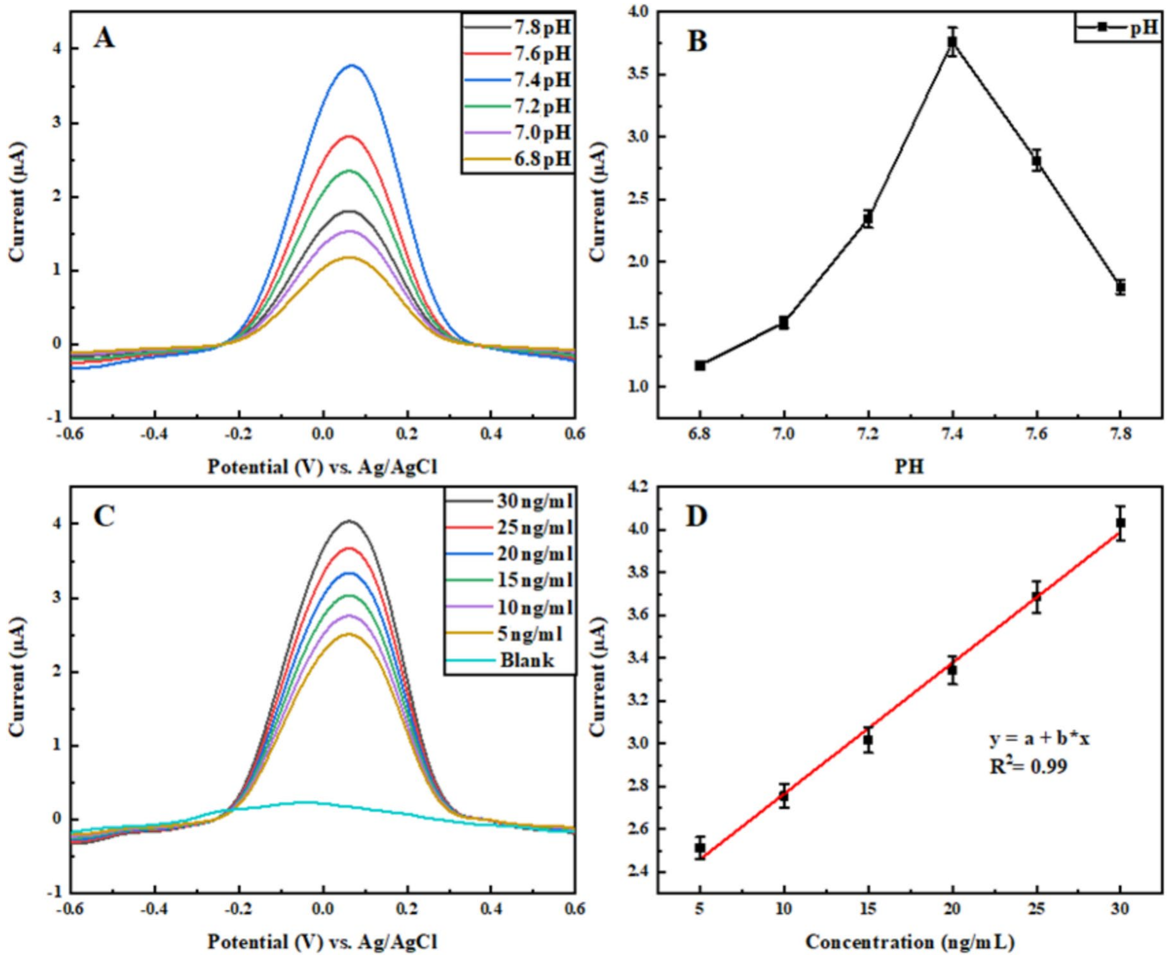

Fig. 4 **A** Differential pulse voltammograms in different pH solutions (6.8–7.8) of 30 ng/mL SVA in 0.1 M PBS, **B** The calibrated line graph between pH and current, **C** Differential pulse voltammograms obtained at different snake venom concentrations (5 ng/mL – 30 ng/mL)and blank reading in 0.1 M PBS, and (**D**) Calibrated line graph between current and concentration

resistance (Rct) was determined. The bare electrode has a surface area of 0.073 cm^2 in 0.1 M potassium ferrocyanide solution and an R_{ct} of 27,659 Ω. Sb_2WO_4@Sm-Co-COOH-MPA-Ab electrode has a higher surface area of 0.145 cm^2 and R_{ct} of 22,018 Ω. Compared to the bare electrode, the modified electrode has reduced R_{ct} (Fig. 6A).

According to EIS in Fig. 6B, the 30 ng/mL concentration has the highest impedance value. Results showed the highest resistance and reactance in the system at this snake venom quantity, indicating the strongest antipathy to current flow. The impedance measurements are carried out with a 30 ng/mL concentration at pH of 6.8, 7.0, 7.2, 7.4, 7.6, and 7.8 (Fig. 6C). The system has the least resistance to current flow at pH 7.4, as indicated by the impedance.

Exponential factor

The following equation calculates the exponential factor:

$$Exponentialfactor = \frac{RT}{R^2 + (2pif \times \tau)^2} \quad (9)$$

R is the charge transfer resistance, pi is the circle's perimeter (~3.14), f is the frequency (0.01 Hz), and τ the time constant. $\tau = R \times C$ where C is the capacitance. The exponential factor for Sb_2WO_4@Sm-Co-COOH with antivenom polyvalent antibodies is 4.5×10^5. It is 3.0×10^7 for bare GCE. The exponential factors for detecting snake venom at optimum pH and concentration (R_{ct} for optimum pH and concentration are 35,219 Ω and 35,453 Ω) are 2.4×10^1 and 2.0×10^1, respectively.

Chronoamperometry

Chronoamperometry evaluates the selectivity, reliability, and stability of the designed immunosensor. The chronoamperometric curve of Sb_2WO_4@Sm-Co-COOH with

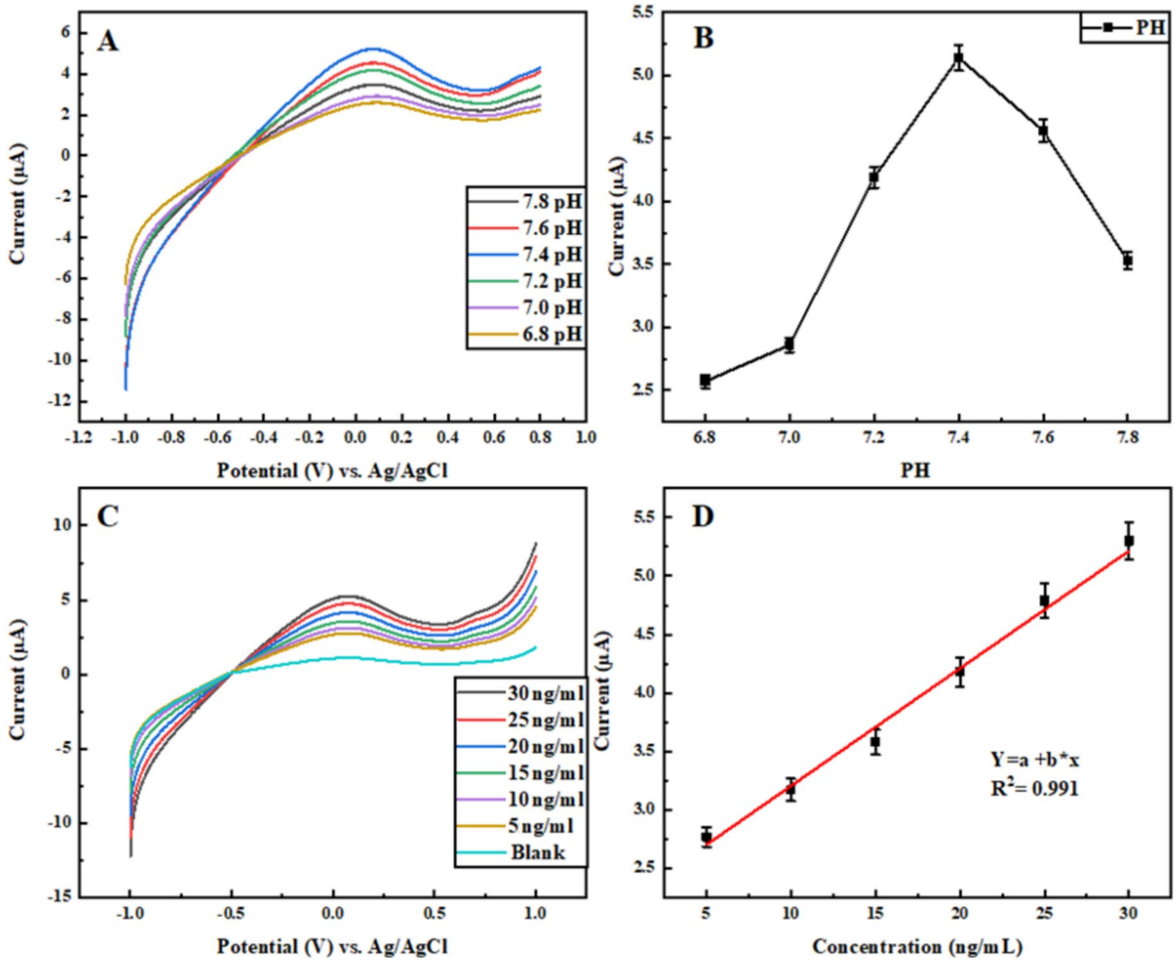

Fig. 5 **A** Linear sweep voltammograms at different pH (6.8–7.4), **B** The calibrated line graph between current and pH at scan rate 30 mVs^{-1}, **C** Linear sweep voltammograms at different snake venom concentrations (5 ng/mL-30 ng/mL) and blank (**D**) The calibrated line graph between current and concentration

antivenom polyvalent antibodies is obtained at a scan rate of 50 mV/s for 14 h. Figure 7A reflects a sudden decrease in current up to 2 h, showing the linear response. The current becomes stable, indicating the immunoreaction kinetics and consistency of the developed immunosensor. An interference study examines the selectivity and stability of immunosensors towards snake venom. The interfering species include proteins, i.e., hemoglobin, albumin, amino acids, cysteine, and tyrosine in PBS solution containing 30 ng/mL snake venom (Fig. 7B). A little drop in immunosensor's current rate towards analyte is seen due to interfering species. The possibility of cross-reactivity was evaluated for these. This experiment showed that these species did not cause significant interference and that the created immunosensor's specificity had increased for selective SVA identification. These analytes do not aggregate with the sensor because of the specific antivenom antibody used in its fabrication.

Amperometric selectivity coefficient

The equation for calculating the immunosensor's amperometric selectivity coefficient is as follows:

$$i_t = K(C_i + \sum k_{ij}^{amp} C_j) \tag{10}$$

where K is the catalytic reaction rate constant (8.1×10^{-7}), Ci is the concentration of the target analyte (30 ng/mL), Cj is the interfering species concentration (30 ng/mL), and ∑kijamp is the amperometric selectivity coefficient. Other species interfere in the amperometric measurement of the target analyte when $\sum k_{ij}^{amp}$ is higher. $\sum k_{ij}^{amp}$ of developed immunosensor is 3.1.

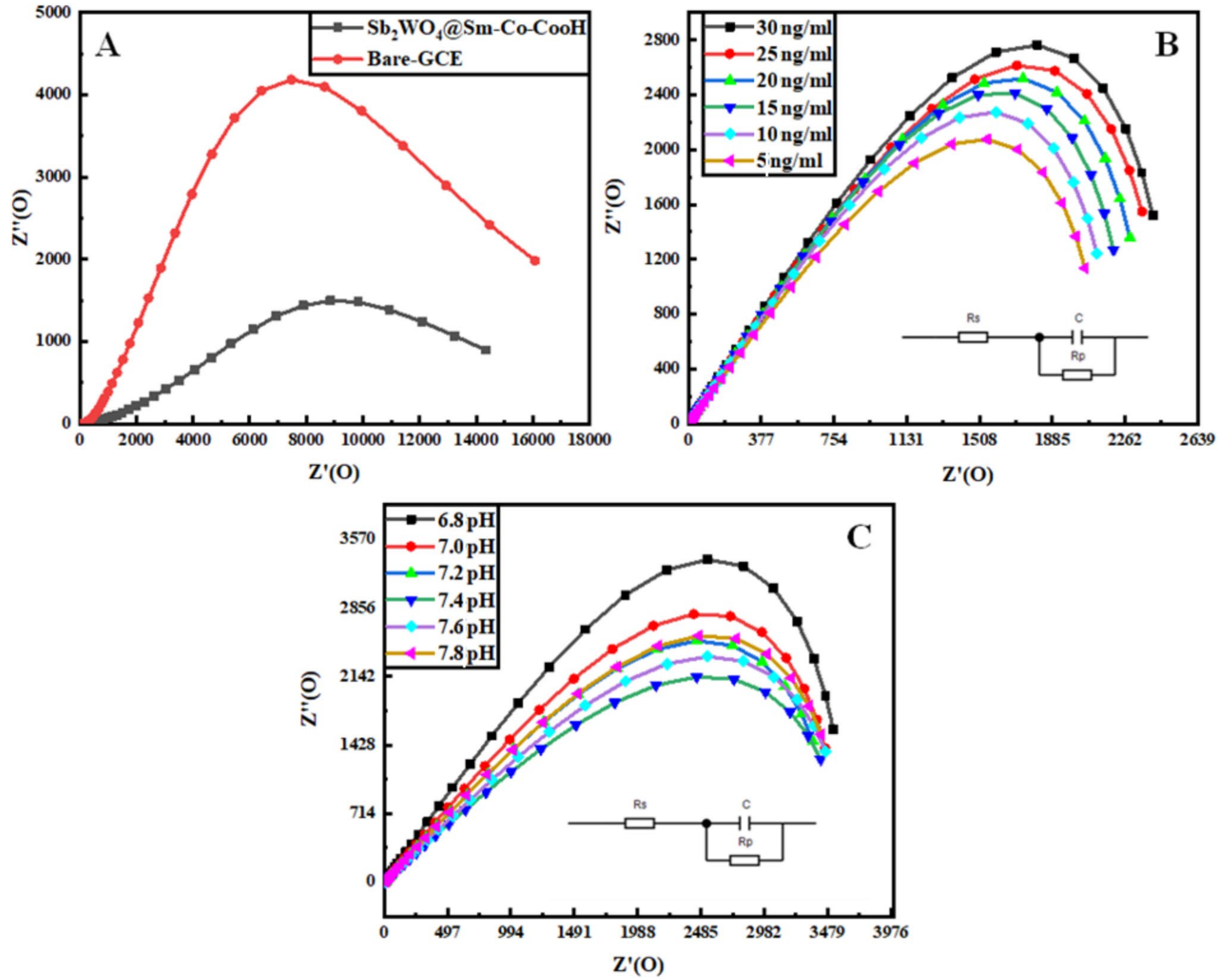

Fig. 6 **A** Electrochemical impedance spectroscopic (EIS) analysis of bare GCE and Sb_2WO_4@Sm-Co-COOH modified electrode, **B** EIS analysis at different snake venom concentrations (5 ng/mL to 30 ng/mL), and (**C**) EIS analysis of snake venom at different pH (6.8–7.8)

Discussion

Sensitive analytical approaches are challenging to develop since human clinical biomarkers are rare. A target analyte and an electrolyte on electrode surfaces undergo a redox reaction, transforming chemical signals into electrochemical signals and is the basis for the electrochemical assay. Also, there is a direct correlation between the analyte concentration and the current intensity. Many clinical biomarkers have been found using this sensitive, quick, and easy procedure. Because of the properties of the electrode materials, the electrochemical assay is preferable (Numan et al. 2021). PtPd nanocubes@MoS_2 "(PtPd@MoS_2)", for detecting Hepatitis B surface antigen (HBs Ag), was presented in a recent study. It produced electrochemical signals. The concentration of HBsAg was detected with a wide linear range of 32 fg mL – 1 to 100 ng mL – 1 and a LOD of 10.2 fg mL – 1 by differential pulse voltammetry (DPV). The purpose of "PdPt@MoO_2" was to detect VEGF with a LOD of 8.2 (pg mL – 1). The response signal of the biosensors has been improved by signal amplification techniques based on antibodies, nucleic acid aptamers, and other enzymes because appropriate recognition molecules and intermolecular forces are essential for high sensitivity and specificity (Liang et al. 2023). Proposing fresh signal amplification approaches coupled with sophisticated procedures is valuable to ensure sensitive and reliable detection of clinical low abundance biomarkers. Building biological interfaces and transferring or amplifying signal molecules are often the mainstays of signal amplification techniques. Biomolecules could be separated and enhanced by biological processes, such as antigen–antibody reactions, to increase sensitivity (Wang et al. 2022).

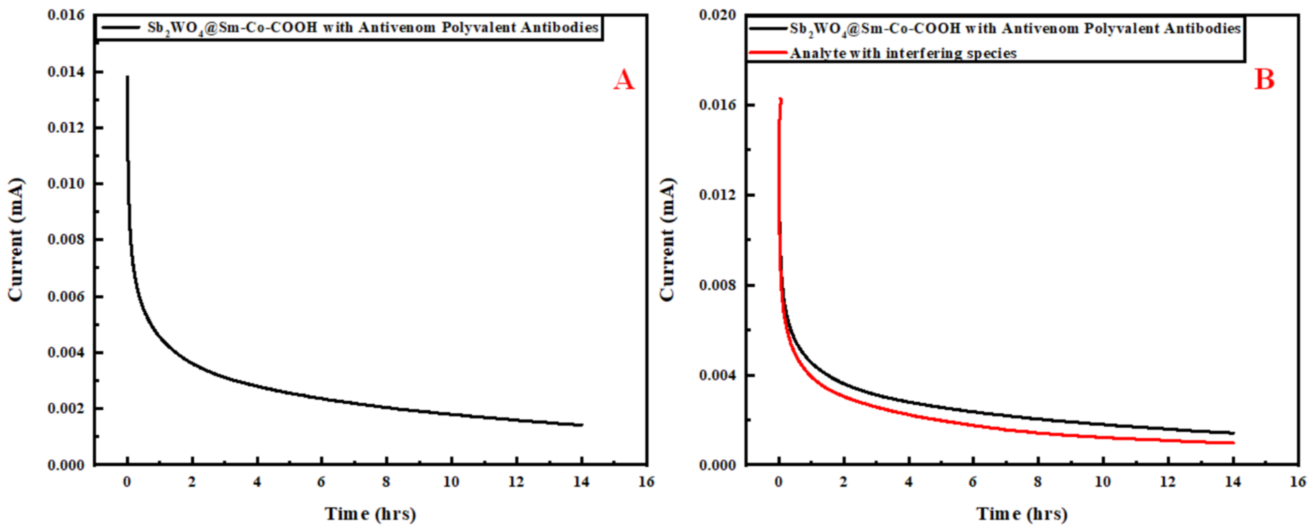

Fig. 7 **A** Chronoamperometric graph of immunosensor Sb_2WO_4@Sm-Co-COOH with antivenom polyvalent antibodies, and (**B**) Interference experiments with various analytes demonstrated the immunosensor's selectivity

The outstanding performance of immunosensors in repeatability and sensitivity suggests that this technology may be helpful and affordable. In an investigation conducted recently, a screen-printed gold electrode (SPGE) biosensor was created to identify *B. candidus* venom in the plasma of rats that were experimentally envenomed (Choowongkomon et al. 2024). According to another investigation, a "TiO_2"-based impedimetric immunosensor was developed to detect snake venom with a detection limit of 20 µg mL^{-1}(de Faria et al. 2019). Another immunosensor that uses the electrochemical impedance spectroscopy method to identify the venoms of Bothrops snakes in particular. To do this, the transducer substrate functionalized with antibothropic antibodies was "Crofer 22 APU steel". The LOD was estimated to be 0.27 µg mL – 1 (de Faria et al. 2018). "Polyaniline-Crofer 22 APU" steel was developed to detect SVA with a LOD of about 0.1 µg/mL (de Faria et al. 2020). 0.08 ng/mL and 0.1 ng/mL range was observed via novel immunosensor of this study. The developed "Sb_2WO_4@Sm-Co-COOH-MPA-Ab" is sustainable and affordable compared to ELISA, which is expensive and has LOD 1–5 ng/mL, 1–3 pg mL^{-1}, 2 ng mL^{-1}, 10 ng mL^{-1} and 7 ng mL^{-1} according to the literature (Puzari and Mukherjee 2020). A detailed comparison of previously reported immunosensors is given in Table 1.

The dense packing of synthesized nano-spheres indicates that Sb_2WO_4@Sm-Co-COOH are agglomerated and have a regular geometry. The size distribution is between 20 and 36 nm, indicating reduced size with higher surface area. The TEM micrograph shows an average diameter of ~ 25 nm. This is due to the homogenous dispersion of Sb, Sm, and Co metals. The absorption wavelength of 214 nm is of Sb_2WO_4@Sm-Co material having OH groups. The deviation of this π to 216 nm is due to the functionalization of the NPs with COOH groups. Sb_2WO_4@Sm-Co-COOH showed a slight change in the band gap, which means that adding carboxyl functional groups did not affect the size or surface characteristics of NPs, and they are highly confined. C-H, C-O–H, and O–H vibrations show the peak positions at 750 cm^{-1}, 1000–1150 cm^{-1}, and 3430 cm^{-1}. The tensile vibration of COOH is responsible for the adsorption peak at 3350 cm^{-1}. Intramolecular hydrogen bonding is the primary cause of the absorption band at approximately 3400 cm – 1 in all nanomaterials (Li et al. 2012). The peak at 500 cm^{-1}

Table 1 Recently developed immunosensors for detecting snake venom, their sensing parameters, linear ranges, and LODs

Sr. No	Immunosensor	Sensing parameter	Linear range	Limit of detection	References
1	Polyaniline-Crofer 22 APU steel	EIS, CV	1–10 µg/mL	0.1 µg/mL	(de Faria et al. 2020)
2	GQDs/nanobody platform	CV	4–20 ng/mL	0.5 ng/mL	(Mars et al. 2018)
3	Au-electrode	CV, EIS	10–400 ng/L	10^{-11} M	(Zehani et al. 2018)
4	CFMs-mesoporous carbon/OHP sheet	CV	50–300 µM	18.98 µM	(Amreen et al. 2022)
5	Sb_2WO_6@Sm-Co-COOH-MPA-Ab/GCE	DPV, LSV, EIS	5–30 ng/mL	0.08–0.1 ng/mL	**Current work**

indicates the presence of metals (M), including Sb, Sm, Co, and W.

The voltammetric analysis of Sb_2WO_4@Sm-Co-COOH-MPA-Ab via CV indicated a potential range of −0.4 to 1.0 V and a scan rate of 30 mVs^{-1}, necessary to bind antibodies successfully. The oxidation peaks at 0.5 V and 35 μA confer the stability and conductivity of the immunosensor. ECSA of immune-electrode indicates a non-conductive area in the potential range of 1.20–1.40 with no oxidation or reduction peaks to reveal little to no electrochemical activity. The ECSA graph shows a relationship between applied potential and resultant current at different scan rates. The maximum current values measured at each scan rate indicate the material's electrochemical activity. The decrease in scan rate alters the electrochemical activity of the immunosensor as no chemical reaction occurs at this point. The non-conductive zone exhibits no oxidation or reduction peaks, indicating no electrochemical process in this potential range. This may be explained by sluggish kinetics in this area, low concentrations of electroactive molecules, or passivation. Rf provides insights into the surface morphology and texture of the modified electrode. The electrochemically active surface area is increased by the electrode modification with Sb_2WO_4@Sm-Co-COOH-MPA-Ab, as seen from the more considerable Rf value of 1.98. The nanocomposite, which is more conductive and promotes increased electron transport between electrode surfaces and analyte solutions, lowers the Rct value. This also indicates improved charge transfer kinetics than bare electrodes. Thus, the electrode's increased surface area creates more electrically active sites to enhance the electrochemical performance. The vast surface area is also attributed to the electrical conductivity of the nanomaterial-modified electrode. The maximum current response of 3.8 μA is obtained at pH 7.4 during DPV measurement. This indicates the electrode works best in pH ranges close to 7.0 because Ab activity decreases in very acidic and basic environments. As the concentration of SVA increases, the peak current also increases. Evidence suggests antigen–antibody complexes are all over the electrode's surface. The specific pH impacts the kinetics of electrochemical reactions due to altered charge transfer mechanism or interaction between immunosensor and snake venom antigen. There is a decrease in electrochemical activity or accessibility of snake venom at lower pH, as seen in the diminishing current peaks. LSV indicated the maximum SVA concentration of about 30 ng/mL because peak current increases with the increase in snake venom concentration. LOD values of 0.08 ng/mL and 0.1 ng/mL are in extraordinary range, which means the fabricated immunosensor can detect the SVA in a small quantity. EIS results show improved charge transfer kinetics, electroactive sites, and thus high electrochemical activity. Therefore, the maximum peak values of pH 7.4 and 30 ng/mL have conducive electrochemical behavior for venom detection. The immunosensor is more sensitive to antigen detection at optimal pH. The interference analysis specified the immunoreaction kinetics and consistency of the developed immunosensor. There is a minimum change in the conductivity of the immunosensor as its activity is not affected by interfering species.

Herein, an Sb-based immunosensor is designed for label-free determination of SVA. Sb_2WO_4@Sm-Co-COOH-MPA-Ab is a novel combination. Antivenom polyvalent antibody is immobilized onto the electrode via MPA in combination with EDC and NHS. This linker improves the Ab conjugation and enhances the electrochemical performance. The synthesized immuno-material enhances the surface area and conductivity of bare GCE. A plethora of functional groups enhance the covalent attachment of SVA to the bioconjugate. Its wide linear range and LOD indicate its capability to detect the low concentrations of the analyte. The size, shape, components, and functional groups of Sb_2WO_4@Sm-Co-COOH are confirmed by FTIR, UV, SEM, and EDS. CV is used to investigate the applicability of immunoconjugate, while DPV, LSV, and EIS detect SVA at various concentrations and pH. Chronoamperometry measures the modified electrode's stability. There is no interference from other analytes, including hemoglobin, albumin, tyrosine, and cysteine. The developed immunosensor exhibits high sensitivity, selectivity, and stability in SVA. It is possible to extend the methodology to less expensive, more sensitive, and selective nanodevices to detect SVA from real biological samples. In addition, it demonstrated outstanding operational stability, exceptional reproducibility, and repeatability. Subsequent investigations ought to concentrate on optimizing the immunodetection technique and utilizing it in the development of a prototype to evaluate its potential in clinical settings. The standard SVA analysis showed that it is appropriate for studying real samples and has excellent precision. It need to be sustainable diagnostic sensor together with the future antivenom production processes. This immunosensor may be used for future point-of-care (POC) testing. According to the research, the created immunosensor may find use in diagnostic clinics for the critical purpose of detecting snake venom on time for medical intervention. To evaluate the effectiveness of this sensor in complicated biological samples and under various conditions, more validation of clinical situations is required. Among the difficulties is the possibility of introducing matrix effects while assessing SVA in actual biological samples, which could impede the detection procedure. A small sample size may have limited the research and impacted how broadly the results may be applied. It does not offer comprehensive insights into the long-term physiological effects of snake venom on survivors; instead, it concentrates on the identification of antigens in snake venom.

Acknowledgements The authors acknowledge the Higher Education Commission (HEC) of Pakistan for their support.

Authors' contribution R.B.: Methodology; Formal analysis, Wrote initial draft.

S.S.: Methodology; Formal analysis.

B.F.: Conceptualization; Supervision; Validation.

D.H.: Validation, Visualization, Wrote final draft.

U.J.: Wrote initial draft.

A.A.: Reviewing; Visualization.

M.N.H: Validation, Visualization, Wrote final draft.

Data availability All the data is included in the manuscript.

Declarations

Ethical approval Ethical approval for snake venom samples was obtained from the university research Ethical Committee Bahauddin Zakariya University, Multan, Pakistan (Biochem D-386/2024).

Conflict of interest The authors declare no conflict of interest.

References

Abbas AK, Lichtman AH, Pillai S (2012) Introduction to the immune system. Cellular and molecular immunology. Séptima edición. Saunders, 733–743

Ahsan H (2022) Monoplex and multiplex immunoassays: approval, advancements, and alternatives. Comp Clin Pathol 31(2):333–345

Amreen K, Salve M, Goel S (2022) Portable electrochemical platform with carbon fibre microelectrodes integrated on an OHP sheet for snake venom analysis. IEEE Trans Nanobiosci 22(1):149–154

Aydin S (2015) A short history, principles, and types of ELISA, and our laboratory experience with peptide/protein analyses using ELISA. Peptides 72:4–15

Blasques RV, Pereira MAA, Mendes AMRV, Filho M, Everton N, Gomes WC, Arenas LT, ... Villis, Mendes PC (2020) Synthesis and characterization of a new ceramic nanomaterial SiO2/NPsSm2O3/C-graphite for the development of electrochemical sensors. Mater Chem Phys 243:122255

Brestoff JR, Frater JL (2022) Contemporary challenges in clinical flow cytometry: small samples, big data, little time. The J Appl Lab Med 7(4):931–944

Chen S, Zhou M, Li T, Cao W (2018) Synthesis of Ag-loaded Sb2WO6 microsphere with enhanced photocatalytic ability for organic dyes degradations under different light irradiations. J Mol Liq 272:27–36

Chen X, Shu W, Zhao L, Wan J (2023) Advanced mass spectrometric and spectroscopic methods coupled with machine learning for in vitro diagnosis. View 4(1):20220038

Choowongkomon K, Chaisakul J, Seetaha S, Vasaruchapong T, Hodgson WC, Rasri N, ... Sookprasert N (2024) Development of a biosensor to detect venom of Malayan krait (Bungarus candidus). Toxins 16(1):56

de Faria RAD, de Freitas Cunha Lins V, Nappi GU, Matencio T, Heneine LGD (2018) Development of an impedimetric immunosensor for specific detection of snake venom. BioNanoScience 8:988–996

de Faria RAD, Houmard M, do Rosário VAM, de FreitasCunhaLins V, Heneine LGD, Matencio T (2019) TiO2 sol-gel coating as a transducer substrate for impedimetric immunosensors. Chem Biochem Eng Q 33(4):437–447

de Faria RAD, de Souza PHC, Lins VDFC, Matencio T, Heneine LGD (2020) Label-free impedimetric immunosensors for detection of snake venoms using polyaniline as a transducer substrate. Biomed J Sci Tech Res 25(3):19083–19091

DeCaprio J, Kohl TO (2020) Immunoprecipitation. Cold Spring Harb Protoc 2020(11):pdb. top098509

Deng X, Zou Z, Zhang Y, Gao J, Liang T, Lu Z, Li CM (2021) Synthesis of merit-combined antimony tetroxide nanoflowers/reduced graphene oxide to synergistically boost real-time detection of nitric oxide released from living cells for high sensitivity. J Colloid Interface Sci 581:465–474

Ghafoor S, Ata S (2017) Synthesis of carboxyl-modified Fe3O4@SiO2 nanoparticles and their utilization for the remediation of cadmium and nickel from aqueous solution. J Chil Chem Soc 62(3):3588–3592

Hu D, Cui H, Wang X, Luo F, Qiu B, Cai W, ... Lin Z (2021) Highly sensitive and selective photoelectrochemical aptasensors for cancer biomarkers based on MoS2/Au/GaN photoelectrodes. Anal Chem 93(19):7341–7347

Kapingidza AB, Kowal K, Chruszcz M (2020) Antigen–antibody complexes. Vertebr Invertebr Respir Protein Lipoproteins Body Fluid Protein 94:465–497

Kirtane AR, Verma M, Karandikar P, Furin J, Langer R, Traverso G (2021) Nanotechnology approaches for global infectious diseases. Nat Nanotechnol 16(4):369–384

Kumar H, Kuča K, Bhatia SK, Saini K, Kaushal A, Verma R, ... Kumar D (2020) Applications of nanotechnology in sensor-based detection of foodborne pathogens. Sensors 20(7):1966

Lahcen AA, Rauf S, Beduk T, Durmus C, Aljedaibi A, Timur S, ... Salama KN (2020) Electrochemical sensors and biosensors using laser-derived graphene: A comprehensive review. Biosens Bioelectron 168:112565

Lee W, Kim H, Jang G, Kim B-G, Yoon Y (2020) Antimony sensing whole-cell bioreporters derived from ArsR genetic engineering. Appl Microbiol Biotechnol 104:2691–2699

Lee L, Samardzic K, Wallach M, Frumkin LR, Mochly-Rosen D (2021) Immunoglobulin Y for potential diagnostic and therapeutic applications in infectious diseases. Front Immunol 12:696003

Leonardo E, Bardales RH, Leonardo E, Bardales RH (2020) Pitfalls in immunocytochemistry. Pract Immunocytochemistry Diagn Cytol 153–163. https://doi.org/10.1007/978-3-030-46656-5_6

Leote RJB, Matei E, Apostol NG, Enculescu M, Enculescu I, Diculescu VC (2022) Monodispersed nanoplatelets of samarium oxides for biosensing applications in biological fluids. Electrochim Acta 402:139532

Li Y-S, Church JS, Woodhead AL (2012) Infrared and Raman spectroscopic studies on iron oxide magnetic nano-particles and their surface modifications. J Magn Magn Mater 324(8):1543–1550

Li Y, Jin L, Chen T (2020) The effects of secretory IgA in the mucosal immune system. Biomed Res Int 2020(1):2032057
Liang D, Wang Y, Qian K (2023) Nanozymes: applications in clinical biomarker detection. Interdisc Med 1(4):e20230020
Lu R-M, Hwang Y-C, Liu I-J, Lee C-C, Tsai H-Z, Li H-J, Wu H-C (2020) Development of therapeutic antibodies for the treatment of diseases. J Biomed Sci 27:1–30
Lutz CS, Hasan AZ, Bolotin S, Crowcroft NS, Cutts FT, Joh E, ... Hayford K (2023) Comparison of measles IgG enzyme immunoassays (EIA) versus plaque reduction neutralization test (PRNT) for measuring measles serostatus: a systematic review of head-to-head analyses of measles IgG EIA and PRNT. BMC Infect Dis 23(1):367
Manohar SM, Shah P, Nair A (2021) Flow cytometry: principles, applications and recent advances. Bioanalysis 13(3):181–198
Mars A, Bouhaouala-Zahar B, Raouafi N (2018) Ultrasensitive sensing of Androctonus australis hector scorpion venom toxins in biological fluids using an electrochemical graphene quantum dots/nanobody-based platform. Talanta 190:182–187
Megha KB, Mohanan PV (2021) Role of immunoglobulin and antibodies in disease management. Int J Biol Macromol 169:28–38
Mourdikoudis S, Pallares RM, Thanh NTK (2018) Characterization techniques for nanoparticles: comparison and complementarity upon studying nanoparticle properties. Nanoscale 10(27):12871–12934
Numan A, Gill AAS, Rafique S, Guduri M, Zhan Y, Maddiboyina B, ... Dang N (2021) Rationally engineered nanosensors: a novel strategy for the detection of heavy metal ions in the environment. J Hazard Mater 409:124493
Oliveira JP, Prado AR, Keijok WJ, Antunes PWP, Yapuchura ER, Guimarães MCC (2019) Impact of conjugation strategies for targeting of antibodies in gold nanoparticles for ultrasensitive detection of 17β-estradiol. Sci Rep 9(1):13859
Orooji Y, Sohrabi H, Hemmat N, Oroojalian F, Baradaran B, Mokhtarzadeh A, ... Karimi-Maleh H (2021) An overview on SARS-CoV-2 (COVID-19) and other human coronaviruses and their detection capability via amplification assay, chemical sensing, biosensing, immunosensing, and clinical assays. Nano-micro Lett 13:1–30
Puzari U, Mukherjee AK (2020) Recent developments in diagnostic tools and bioanalytical methods for analysis of snake venom: a critical review. Anal Chim Acta 1137:208–224
Rabiei M, Palevicius A, Monshi A, Nasiri S, Vilkauskas A, Janusas G (2020) Comparing methods for calculating nano crystal size of natural hydroxyapatite using X-ray diffraction. Nanomaterials 10(9):1627
Rafiq U, Mehraj O, Lone S, Wahid M, Majid K (2020) Solvothermal synthesis of Ag2WO4/Sb2WO6 heterostructures for enhanced charge transfer properties and efficient visible-light-driven photocatalytic activity and stability. J Environ Chem Eng 8(5):104301
Rasouli Jamnani S, Milani Moghaddam H, Leonardi SG, Donato N, Neri G (2019) Samarium oxide as a novel sensing material for acetone and ethanol. Paper presented at the Sensors: Proceedings of the Fourth National Conference on Sensors, February 21–23, 2018, Catania, Italy 4
Rhiel L, Becker S (2021) Applications of antibodies in therapy, diagnosis, and science. Introduction Antibody Eng 129–159. https://doi.org/10.1007/978-3-030-54630-4_6
Saxena K, Kumar A, Chauhan N, Khanuja M, Malhotra BD, Jain U (2022) Electrochemical immunosensor for detection of H. pylori secretory protein vaca on g-c3n4/ZnO nanocomposite-modified au electrode. ACS Omega 7(36):32292–32301
Schacht V, Kern JS (2015) Basics of immunohistochemistry. J Investig Dermatol 135(3):1–4
Schroeder HW Jr, Cavacini L (2010) Structure and function of immunoglobulins. J Allergy Clin Immunol 125(2):S41–S52
Shen Y, Zhang Y, Gao ZF, Ye Y, Wu Q, Chen H-Y, Xu J-J (2021) Recent advances in nanotechnology for simultaneous detection of multiple pathogenic bacteria. Nano Today 38:101121
Tan WCC, Nerurkar SN, Cai HY, Ng HHM, Wu D, Wee YTF, ... Lim TKH (2020) Overview of multiplex immunohistochemistry/immunofluorescence techniques in the era of cancer immunotherapy. Cancer Commun 40(4):135–153
Wang Y, Li B, Tian T, Liu Y, Zhang J, Qian K (2022) Advanced on-site and in vitro signal amplification biosensors for biomolecule analysis. TrAC, Trends Anal Chem 149:116565
Zehani N, Cheewasedtham W, Kherrat R, Jaffrezic-Renault N (2018) Impedimetric biosensor for the determination of phospholipase A2 activity in snake venom. Anal Lett 51(3):401–410
Zhang Y, Liu D, Zhang Y, Qian Y, Li C, Qu Z, ... Wei Q (2022) Highly sensitive photoelectrochemical neuron specific enolase analysis based on cerium and silver Co-Doped Sb2WO6. Biosens Bioelectron 203:114047
Zhuang Y, Zhang X, Chen Q, Li S, Cao H, Huang Y (2019) Co3O4/CuO hollow nanocage hybrids with high oxidase-like activity for biosensing of dopamine. Mater Sci Eng, C 94:858–866